Electronic structure and optical, mechanical, and transport properties of the pure, electron-doped, and hole-doped Heusler compound CoTiSb

Siham Ouardi, Gerhard H. Fecher,* and Claudia Felser
Institut für Anorganische und Analytische Chemie, Johannes Gutenberg - Universität, 55099 Mainz, Germany and Max Planck Institute for Chemical Physics of Solids, D-01187 Dresden, Germany

Michael Schwall, S. Shahab Naghavi, Andrei Gloskovskii, and Benjamin Balke
Institut für Anorganische und Analytische Chemie, Johannes Gutenberg - Universität, 55099 Mainz, Germany

Jaroslav Hamrle, Kamil Postava, and Jaromír Pištora
Department of Physics and Nanotechnology Center, VSB - Technical University of Ostrava, 70833 Ostrava-Poruba, Czech Republic

Shigenori Ueda
Synchrotron X-ray station at SPring-8, National Institute for Materials Science, Hyogo 679-5148, Japan

Keisuke Kobayashi
NIMS Beamline Station at SPring-8, National Institute for Materials Science, Hyogo 679-5148, Japan
(Received 21 April 2012; published 16 July 2012)

The Heusler compound CoTiSb was synthesized and investigated theoretically and experimentally with respect to electronic structure and optical, mechanical, and vibrational properties. The optical properties were investigated in a wide spectral range from 10 meV to 6.5 eV and compared with *ab initio* calculations. The optical spectra confirm the semiconducting nature of CoTiSb, with a strong exciton absorption at 1.83 eV. The calculated phonon dispersion as well as elastic constants verify the mechanical stability of CoTiSb in the cubic $C1_b$ system. Furthermore, solid solution series of $CoTi_{1-x}M_xSb$ (M = Sc, V and $0 \leqslant x \leqslant 0.2$) were synthesized and investigated. The transport properties were calculated by all-electron *ab initio* methods and compared to the measurements. The thermoelectric properties were investigated by measuring the temperature dependence of electrical resistivity, Seebeck coefficient, and thermal conductivity. The thermal conductivity of the substituted compounds was significantly reduced. Sc substitution resulted in a p-type behavior with a high Seebeck coefficient of $+177.8\ \mu$V/K (350 K) at 5% Sc substitution. This value is in good agreement with the calculations. Fully relativistic Korringa–Kohn–Rostoker calculations in combination with the coherent potential approximation clarify the different contribution of states in the (001) plane of the Fermi surface for Sc- or V-substituted compounds $CoTi_{0.95}M_xSb$ (M = Sc, V).

DOI: 10.1103/PhysRevB.86.045116 PACS number(s): 71.23.−k, 78.20.−e, 72.15.−v

I. INTRODUCTION

Heusler compounds with the general formula $TT'M$ (where T and T' are transition metals and M is a main group element) and a 1 : 1 : 1 composition are ordered in $C1_b$ structure that consists of an fcc lattice where three of the four positions with highest symmetry (T_d) in the primitive cell are occupied and the fourth is left vacant. The properties of these $TT'M$ compounds depend strongly on the valence electron concentration (VEC) or number of valence electrons (N_v) in the primitive cell, which determine the band structure and accordingly the physical properties of the compounds.[1,2] Compounds with $N_v = 21$, or 22 like NiMnSb, were suggested to be halfmetallic ferromagnets.[3] Compounds with $N_v = 20$ are not stable due to the localization of the Fermi level ϵ_F at states of the antibonding region.[2] In particular, compounds with $N_v = 18$ exhibit a closed shell type behavior with filled bands (a_1, t_2, e, t_2) and therefore are found to be semimetals or semiconductors.[1] Compounds containing *heavy* metals (Au, Pt, Sb, or Bi) and a lanthanide element often exhibit a *zero band gap* state. They are so-called gapless semiconductors. That is, the band gap is closed through the touching of the valence and conduction bands at ϵ_F. According to the earlier electronic structure computations,[4] several materials with a zero direct gap at Γ were predicted to be on the borderline to topological insulators. From previous band structure calculations and experimental studies, it is concluded that numerous 18 VEC-Heusler systems based on *light* transition metals (likewise CoTiSb or FeVSb) exhibit semiconducting properties, with narrow band gaps in the density of states (DOS).[1,2] The value of the gap in these compounds is related, to a large extent, to the hybridization between d states of the transition metals T and T'.[5] These narrow-band-gap compounds were reported to exhibit excellent thermoelectric properties[6,7] due to wide possibilities of modifying their electronic properties by partial substitution or doping.

Since the first investigation as semiconductor by Kouacou and coworkers,[8] CoTiSb has attracted a considerable interest as a promising candidate for thermoelectric applications. Up to today, there are more than thirty investigations that are focused on CoTiSb-based compounds, concerning band structure calculations,[1,2,5,9–12] synthesis,[13] disorder,[14–17] magnetism,[18–20] and thermoelectric properties.[21–30] The best

p-type thermoelectric properties for Heusler compounds were achieved in CoSb-based materials.[26,29] Recently, the highest thermoelectric figure of merit ZT of 0.8 at 700 °C was observed for the *p*-type Heusler compound $CoZr_{0.5}Hf_{0.5}Sb_{0.8}Sn_{0.2}$.[31] These promising behaviors enhance intensive theoretical and experimental studies of the CoTiSb compound.

On the other hand, the study of the optical and mechanical properties were reported as a useful method to investigate the band gap[32–35] and stability of some Heusler compounds.[36–38] Most recent studies focused on the optimization of the thermoelectric properties, such as nanostructuring to minimize thermal conductivity, or partial atom substitution to decrease electrical conductivity and/or increase the Seebeck coefficient. Measurements of optical properties have been applied rarely and investigations of mechanical properties have been neglected, so far.

In the present study, the optical properties of CoTiSb measured by spectroscopic ellipsometry and Fourier transform infrared spectroscopy were investigated and compared to an *ab initio* calculation. The stability of the compound was studied by investigation of mechanical properties and phonon calculations. The electronic structure of CoTiSb and Sc and V substitution of Ti was investigated by means of hard x-ray photoelectron spectroscopy (HAXPES) and compared to the calculations. The influence of site disorder on the electrical conductivity of CoTiSb was investigated by *ab initio* calculations and compared to experiments. Furthermore, the effect of Ti substitution by Sc and V on the thermoelectric properties of the Heusler compounds $CoTi_{1-x}M_xSb$ (where M = Sc, V and $0 < x \leqslant 0.2$) was investigated and compared to theoretical predictions.

II. DETAILS OF THE CALCULATIONS

Electronic structure and optical and transport properties of the compounds were calculated by the full potential linearized augmented plane wave (FLAPW) method as implemented in WIEN2k[39] in combination with a modified version of BOLTZTRAP[40](for details see Ref. 41). The calculations were performed in the semirelativistic mode by solving the Dirac equation only for core states and neglecting spin-orbit interaction for the valence states. The exchange-correlation functional was taken within the generalized gradient approximation (GGA) in the parametrization of Perdew, Burke, and Enzerhof (PBE).[42] For integration, a $31 \times 31 \times 31$ point mesh was used resulting in 816 k points in the irreducible wedge of the Brillouin zone. The energy convergence criterion was set to 10^{-5} Ry and simultaneously the criterion for charge convergence to $10^{-3}e^-$. Relaxed lattice parameters were used in all calculations, the optimization of the volume resulted in $a = 5.8981$ Å for CoTiSb. Details of calculations are described in Ref. 41.

The calculation of the electronic structure of disordered or substituted compounds is more demanding compared to the pure compounds because of noninteger site occupancies accompanied by the loss of periodicity of the crystalline structure. One approach is the use of supercells with a large number of sites. This allows to model vacancies by removal of atoms in the supercell or antisite disorder by changing the positions of selected atoms. Substituted compounds may be described by exchanging kinds of atoms on fixed sites. A drawback is that the calculations can be performed only for fractional types of site occupancies ($x = i/n$, $i < n$) that depend on the total number of sites (n) in the supercell. In the present work, two alternative approaches were used that allow for nonrational site occupancies x. One is the virtual crystal approximation (VCA) that can be performed within the FLAPW method. In the VCA, the atoms are replaced by "virtual" elements that have different (noninteger) nuclear charges and numbers of valence electrons. It is suited for small amounts ($x \ll 1$) of substituted atoms that are (neighboring) in the same row of the periodic table of elements. The other method used here—and allowing to replace "real" element—is the coherent potential approximation (CPA) that can be performed within the Korringa–Kohn–Rostoker (KKR) Green's function method. In the CPA, the random array of real on-site potentials is replaced by an ordered array of effective potentials and thus it describes the behavior of an atom in a mean-field environment. The CPA is suited for any site occupation $0 < x < 1$. The disadvantage of both VCA and CPA is that they do not include the local environment effects such as preferential ordering or lattice relaxations around the impurity site.

The electronic structure of substitutionally disordered $CoTi_{1-x}M_xSb$ (where M = Sc, V and $0 < x \leqslant 0.2$) was calculated by means of the VCA. The substitution of Ti by an amount x of Sc or V results in a reduction or an addition by $x\ e^-$ because the difference in the valence electrons of those atoms is ± 1. Therefore the charge and number of electrons at the Ti site (4c) of CoTiSb was set to $(22 \pm x)\ e^-$ to model the $Co(Ti_{1-x}M_x)Sb$ (M = Sc, V) solid solutions. It should be noted that the VCA method has the drawback that it is not element specific. This means that the result would be the same for $CoTi_{1\pm y}Sb$ or any suitable substitution by other elements resulting in the same valence charge. The resulting band structure is also an approximation as it is absent in real solid solutions with random site occupation and thus a missing periodicity of the crystalline structure.

Furthermore, the electronic structure calculations of CoTiSb with antisite disorder and substituted $CoTi_{1-x}M_xSb$ (where M = Sc, V and $0 < x \leqslant 0.2$) have been performed by means of the fully relativistic KKR method in combination with the CPA as implemented in the MUNICH-SPRKKR program package.[43] The calculations were performed in the fully relativistic mode by solving the Dirac equation for core and valence states. The k-integration mesh was set to a size of $28 \times 28 \times 28$ during the self-consistent cycles (1128 k points in the irreducible wedge of the Brillouin zone). The gradient correction of the PBE-functional was switched off for the vacant site to avoid numerical instabilities caused by low charge densities. The Co atoms are placed on the 4a Wyckoff position, the Ti atoms are placed together with the M atoms on the 4c position, and the main group element Sn is finally placed on the 4d position. The swap-type disordered CoTiSb [here $Co(Vc_{1-x}Ti_x)(Ti_{1-x}Vc_x)Sb$] compound was also treated using the CPA method by placing a fraction of x vacancies (Vc) on the regular Ti site (4c) and simultaneously the swapped Ti part $(1 - x)$ on the 4b Wyckoff position.

III. EXPERIMENTAL DETAILS

The solid solution series $CoTi_{1-x}M_xSb$ (M = Sc, V and $x = 0, \ldots, 0.2$) was prepared by arc melting. To compensate the loss of the Sb during arcmelting an excess of 5% Sb was used. The ingots were wrapped in tantalum foil and annealed at 900 K for 10 days under argon in quartz ampules. The annealing was followed by slow cooling to room temperature. The ingots were cut to disks and polished for investigations of composition, optical properties, and electronic structure.

The crystalline structure, homogeneity, and composition of the samples were checked by x-ray diffraction (XRD) and energy-dispersive x-ray (EDX) spectroscopy. Powder XRD revealed single phases with $C1_b$ structure for all compounds. The powder XRD experiments were performed by using a Siemens D5000 diffractometer with Cu K_α radiation, $\lambda = 1.5418$ Å, in Bragg geometry. A scanning electron microscope (SEM) (Jeol JSM-6400) equipped with an EDX detection system was used to proof the quality and the distribution of the constituent elements at the surface. The samples were measured in vacuum with a residual pressure of about 3.0×10^{-6} mbar. The primary electron beam had an energy of 20 keV and the EDX detector was mounted at an angle of 35° to the sample surface normal.

The optical investigations were performed using a spectroscopic ellipsometer (Horiba Jobin Yvon, UVISEL) in the energy range 0.6–6.5 eV and Fourier transform infrared (FTIR) spectrometer (Bruker, Vertex 70v) for 6 meV–1 eV. All optical investigations were carried out at room temperature. The ellipsometry data were measured at incidence angles of 60° and 70°. The dielectric function of CoTiSb was obtained from the ellipsometry spectra by eliminating of surface roughness using a 5.2-nm-thick surface layer of an effective medium with 50% of voids. The infrared reflectivity was measured at an incidence angle of 11°.

Transport and specific heat measurements were performed by means of a physical properties measurement system (PPMS; Quantum Design). For transport measurements, sticks of $2 \times 2 \times 8$ mm^3 were cut from the ingots. For the specific heat measurements, small sample pieces of approximately 8 mg were used. The temperature was varied from 1.8 to 350 K. All measurements were performed at a residual pressure of about 9.0×10^{-5} mbar in the PPMS chamber.

For the HAXPES measurements the sample sticks were fractured *in situ* in the ultrahigh vacuum (UHV) chamber before each measurement to avoid contamination when exposed to air. The sticks were identical to those used for the transport measurements. The HAXPES experiments were performed at beamline BL15XU[44] of SPring-8 (Japan). The photon energy was fixed at 5.9534 keV using a Si 111 double crystal monochromator and the 333 reflection of a Si channel-cut post monochromator. The photoelectrons were analyzed and detected by means of a hemispherical analyzer (VG Scienta R4000). The overall energy resolution (monochromator plus analyzer) was set to 140 meV, as verified by spectra of the Au valence band at the Fermi energy (ϵ_F). The angle between the electron spectrometer and photon propagation is fixed at 90°. A near-normal emission angle ($\theta \approx 2°$) was used for electron detection. The measurements were taken at a sample temperature of 20 K.

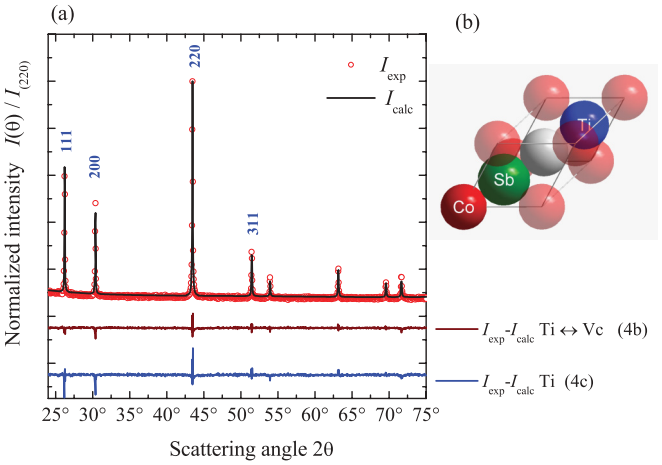

FIG. 1. (Color online) Crystalline structure of CoTiSb. (a) The x-ray diffraction data and results of the Rietveld refinement for ordered and partially disordered CoTiSb. The data were taken at room temperature using Cu K_α radiation. (b) The primitive cell of CoTiSb in the $C1_b$ structure. The light sphere in the center represents the vacancy.

IV. RESULTS AND DISCUSSION

A. Structure and composition

The experiments revealed that pure CoTiSb samples have the correct 1:1:1 stoichiometry and the $C1_b$ structure. Figure 1(b) shows the primitive cell of cubic face centered CoTiSb. The $C1_b$ structure exhibits a vacant site (Vc) in the 4*b* Wyckoff position [the light sphere in the center at $(\frac{1}{2}, \frac{1}{2}, \frac{1}{2})$]. Co, Ti, and Sb occupy the 4a, 4d, and 4c Wyckoff positions at (0,0,0), $(\frac{3}{4}, \frac{3}{4}, \frac{3}{4})$, and $(\frac{1}{4}, \frac{1}{4}, \frac{1}{4})$, respectively. The space group is $F\bar{4}3m$ and the primitive cell as well as the vacant and all three occupied Wyckoff positions have T_d point group symmetry. A Rietveld refinement of the x-ray powder diffraction of CoTiSb is shown in Fig. 1(a). The refinement has the lowest R value ($\leqslant 2.7\%$) when assuming a 3.7 % swap of Ti atoms into the vacant position Vc. Assuming other types of antisite disorder resulted in considerably larger R values. The lattice parameter determined from powder XRD is $a_{exp} = 5.884$ Å. The observed value is in good agreement with those reported previously.[5,18] It is slightly smaller (0.2%) compared to the optimized lattice parameter as is typical for calculations using GGA. The difference is too small to have a noticeable impact on the result of the calculations reported in the following.

Figure 2(a) shows a SEM micrograph of polished CoTiSb recorded over a large area. No evidence of other phases or faults (as for example cracks or inclusions) was observed. The compositional homogeneity checked by the corresponding EDX line scan is show in Fig. 2(b). A uniform distribution of the elements consistent to the microstructure is observed. The results of the quantitative chemical analysis are presented in Table I. CoTiSb shows a 1 : 1 : 1 composition within the experimental uncertainty.

B. Electronic Structure and Optical Properties

Figure 3 compares the band structure of pure CoTiSb to the cases of electron lack and excess at the Ti site calculated in

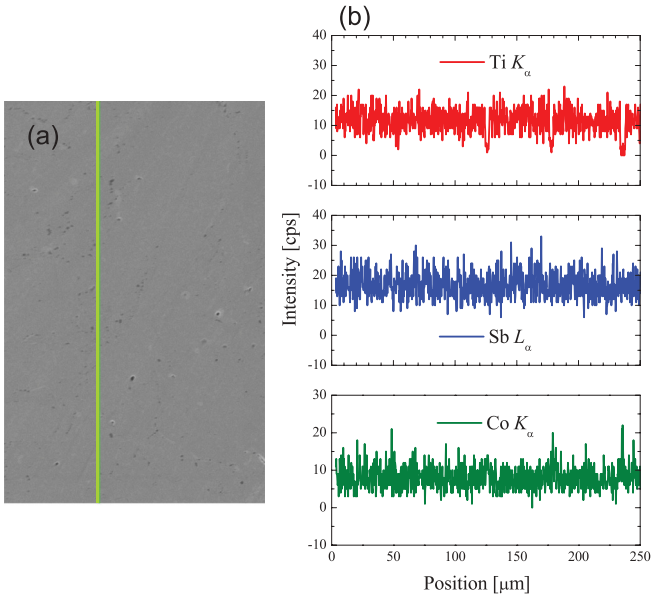

FIG. 2. (Color online) EDX measurement of CoTiSb. (a) SEM micrograph and (b) intensities of characteristic x-ray emission of Ti K_α, Sb L_α, and Co K_α along the line scan.

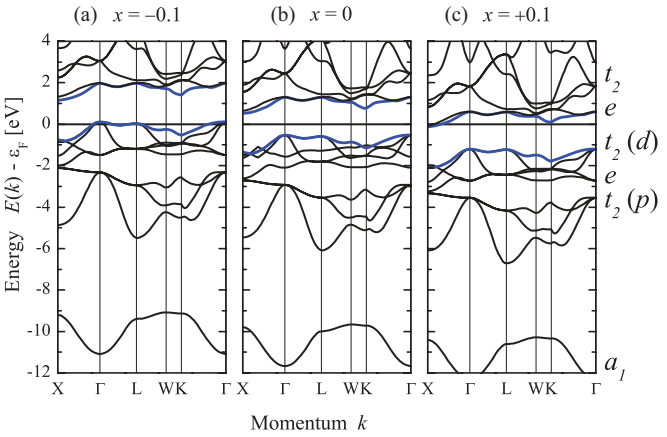

FIG. 3. (Color online) Band structure of CoTiSb with $(22 \pm x)$ e^- ($x = 0,0.1$). The calculations were performed using FLAPW with VCA. The irreducible representations of the states at Γ are marked in (c).

VCA. The topmost valence band at ϵ_F of the semiconducting pure CoTiSb ($x = 0$) has t_2 character at the Γ point that has T_d symmetry. It is followed by d bands of e (−1.56 eV) and bands of t_2 (−2.39 eV) character. The low lying a_1 states are found below −9.4 eV and are separated from the higher lying bands by the sp hybridization gap that is typical for Heusler compounds. The pure CoTiSb exhibits an indirect Γ-X band gap of about 1.06 eV, whereas the optical gap at Γ is considerably larger (1.83 eV). Both, topmost valence band and lowest conduction band appear very low dispersing with a bandwidth of ≈150 meV in the Γ-L direction and thus allow easily for direct optical transitions at energies of about 1.8 eV.

The variation of the number of valence electrons results in an emptying or filling of the valence or conduction bands, respectively. The result is a shift of the ϵ_F into the valence ($x < 0$) or conduction ($x > 0$) bands. Due to the high density of states already close to both band edges this energy shift is only small. At a doping level of $x = \pm 0.1$, ϵ_F is located about 110 meV below or 115 meV above the valence or conduction band edges. The gap is kept with the same size when adding or removing electrons and the change of the electronic structure appears to be of *rigid-band* type, that is, no major changes in the dispersion are observed here when using the VCA approach.

The optical properties of pure CoTiSb are presented in Fig. 4. The spectral dependence of the complex permittivity $\varepsilon = \varepsilon_r + i\varepsilon_i$ is shown in Fig. 4(a). The dominant feature of those spectra is a strong absorption peak at 1.80 eV. This value is in perfect agreement with the direct band gap at Γ and the distance between the flat valence and conduction bands in the Γ-L direction as shown in Fig. 3(b). For energies below 1.8 eV, the optical absorption (ε_i) quickly drops to zero, as expected for semiconductors when the photon energies become smaller than the gap size. The experimentally determined spectra are compared with the results of the *ab initio* calculations. The main features are well reproduced. The position and strength of the optical absorption peaks for energies above 2 eV, namely, at around 3.2 and 5.0 eV, agree well between experimental data and the *ab initio* calculations.

The wide range infrared reflectivity is presented in Fig. 4(b), measured from 10 meV (far infrared) to 1 eV (near infrared). The dominant feature is a strong absorption peak at about 34 meV, where the reflectivity changes abruptly from 100% to 30%. There is also one small absorption peak observed at about 28 meV [see inset in Fig. 4(b)].

TABLE I. Chemical composition of CoTiSb.

Atom	Co	Ti	Sb
Fraction	1.01 ± 0.03	1.00 ± 0.03	0.99 ± 0.03

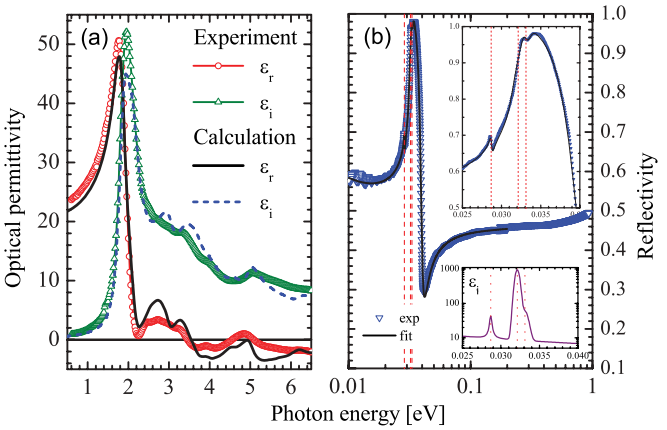

FIG. 4. (Color online) Optical properties of CoTiSb. (a) compares the calculated and measured real ε_r and imaginary ε_i parts of the permittivity, and the infrared reflectivity is shown in (b). Red dashed lines show positions of resonance peaks. Bottom inset in (b) is imaginary part of the permittivity in the infrared region. The calculations in (a) were performed using FLAPW.

In order to describe the reflectivity in detail, the following contributions to the permittivity are used for a fit of the data:

$$\varepsilon = \varepsilon_\infty + \varepsilon_{\mathrm{Dru}} + \sum_{j=1}^{3} \varepsilon_{\mathrm{GL},j}. \quad (1)$$

The term ε_∞ describes the shift of the real part of the permittivity due to photon absorption at higher photon energies. The Drude term originates from the presence of free electrons: $\varepsilon_{\mathrm{Dru}}(E) = E_D^2/(-E^2 - i\gamma E)$, where E_D and γ are the plasma and damping energies, respectively. The fit provides a rather week Drude term with $E_D = 250$ meV and $\gamma = 223$ meV. This corresponds to a quasistatic conductivity of $\sigma = (E_D^2\varepsilon_0)/(\gamma\hbar) = 3.8 \times 10^3$ Sm^{-1}. This rather low optical conductivity reflects the semiconducting nature of CoTiSb (ε_0 is the vacuum permittivity and $\hbar$ is the Planck's constant). The last three terms $\varepsilon_{\mathrm{GL},j}$ correspond to resonant phonon vibrations and are described using Gauss-Lorentzian (Voigt) oscillators.[45]

The dominant peak at $E_{0,1} = 32.1$ meV and two minor peaks at $E_{0,2} = 33.1$ meV and $E_{0,2} = 28.7$ meV describe the main features of the infrared spectra [bottom inset in Fig. 4(b)]. The fit reveals that those absorption peaks are very sharp, with quality factors of $E_0/\gamma > 100$. The peaks originate from absorption of optical phonons (compare Fig. 8). Similar absorption peaks were observed at photon energies of 16.7 and 23.8 meV in PtYSb[46] or at 15.3 and 21.1 meV in NiHfSn.[34]

C. Hard x-ray valence band photoelectron spectroscopy

The electronic structures of CoTiSb, $CoTi_{0.95}Sc_{0.05}Sb$, and $CoTi_{0.9}V_{0.1}Sb$ were investigated by HAXPES. The spectra were taken at 20 K sample temperature with an excitation energy of about 6 keV. Figure 5 compares the calculated total and partial DOS of CoTiSb to the measured valence band spectra. The valence band spectrum with five maxima exhibits the typical structure of Heusler compounds with $C1_b$ structure.[11,41,46,47] In the present work, those states are clearly and much better resolved compared to previous investigations of the valence band of CoTiSb.[11,19] Cause is the much higher resolution ($\Delta E = 140$ meV) of the high brilliant photon source at SPring-8.

All major structures observed in the spectrum are in well agreement to the calculated DOS (see also Fig. 3 for the irreducible representations of the states at the Γ point). The low lying maximum at about −11.5 eV below ϵ_F arises from a_1 (s) states localized at the main group element Sb. Compared to the partial DOS, the peaks at −1.6, −2.3, and −4.0 eV arise mainly from different d states with t_2 or e character located at Co and Ti. The peaks at about −6.9 eV arises mainly from t_2 (p) states. The peaks close to ϵ_F are sharper, as those lying farther away from ϵ_F. This is due to the lifetime broadening that increases with increase of the binding energy. Furthermore, the intensity ratios of the peaks are different from the calculated DOS. This deviation arises from the different partial cross sections of the s, p and d states located at different atoms. Both cross section and lifetime effects are discussed in more detail in Ref. 11.

A large amount of states inside of the semiconducting gap is obvious from Fig. 5(d). In Sec. IV A, the evidence for a Ti↔Vc type antisite disorder of about 4% was found by XRD. As reported previously,[19,41] the occupation of the vacant site of the $C1_b$ structure by one of the constituents while keeping the 1 : 1 : 1 stoichiometry leads to the occurrence of in-gap states. KKR-CPA calculations were performed to explain and analyze the influence of Ti↔Vc antisite disorder on the electronic structure. The results for 5% swap of Ti atoms into the vacant site at fixed, ideal 1 : 1 : 1 stoichiometry are shown in Fig. 6. The details for other types of antisite disorder are explained in Appendix A.

A band structure is not longer defined in disordered or substituted systems with random site occupancies due to the lack of periodicity. However, the density of states and the Bloch spectral function can still be calculated by Green's function methods. The antisite disorder causes a broadening of the initial band dispersion as is seen from the Bloch spectral

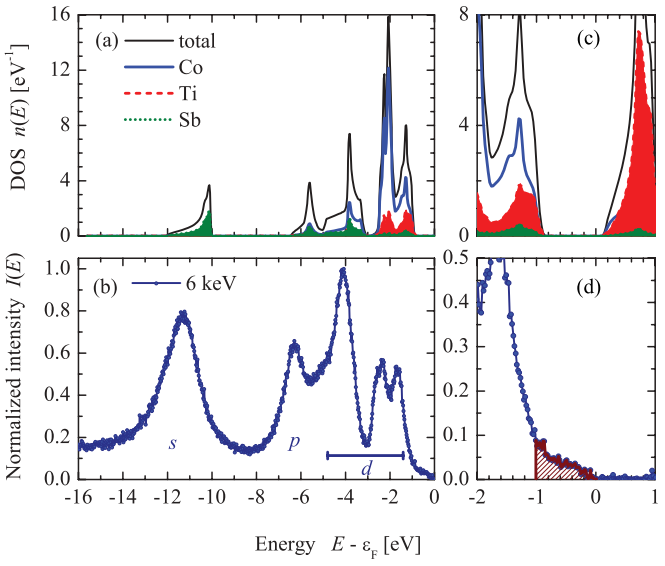

FIG. 5. (Color online) Total and partial density of states (a) and (c) and valence band spectra (b) of CoTiSb. The excitation energy was fixed to 5.9534 keV. The DOS was calculated by FLAPW. The in-gap states are marked by the shaded area in (d).

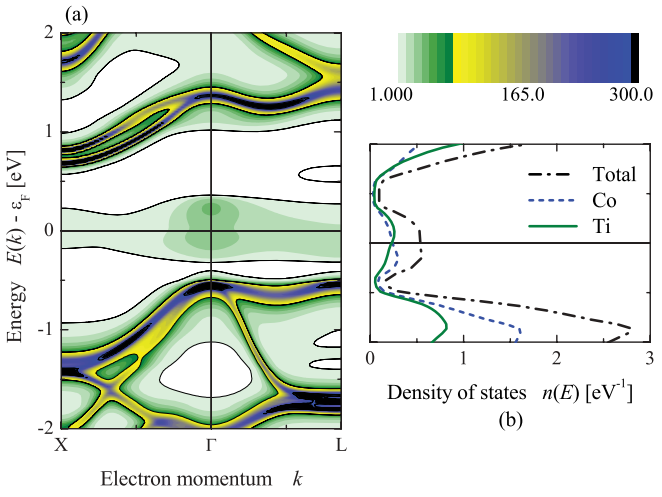

FIG. 6. (Color online) Electronic structure of CoTiSb with 5% Ti↔Vc antisite disorder. (a) Bloch spectral function in the Δ (Γ − X) and Λ (Γ − L) directions. (b) shows the accompanied total and partial density of states calculated for the full Brillouin zone.

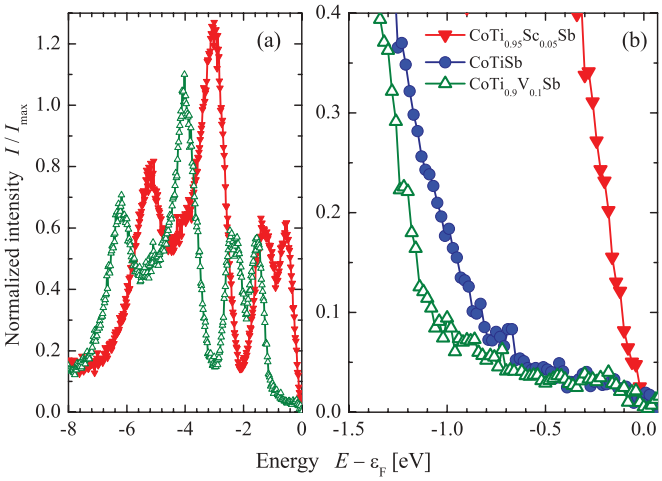

FIG. 7. (Color online) Valence band spectra of substituted CoTiSb. (a) shows the valence bands of $CoTi_{0.95}Sc_{0.05}Sb$ and $CoTi_{0.9}V_{0.1}Sb$ in the range of the d states and (b) the energy range close to ϵ_F on an enlarged view (CoTiSb is included for comparison).

function in comparison to the initial band structure. The course of the major features is the same for the KKR-CPA and the FLAPW-VCA calculations, in particular, there are no mentionable differences in the energies between valence and conduction states. Different from the original band structure, now one recognizes states in the initial band gap that are found around the Γ point and thus are strongly localized as expected for impurity states. The states exhibit a low dispersion but are found over a rather wide band of energies inside of the initial semi-conducting band gap. The orbital momentum analysis of the DOS reveals that those in-gap states have d character. It is interesting to note that the in-gap states below ϵ_F are to a large amount localized at the Co atoms, whereas those above ϵ_F are to a larger amount localized at both Ti atoms in the original 4d as well as the vacant 4b position [see Fig. 6(b)]. That is, they are split of from the former valence or conduction band edges.

Figure 7 compares the measured valence band spectra of the Sc ($CoTi_{0.95}Sc_{0.05}Sb$) and V ($CoTi_{0.9}V_{0.1}Sb$) substituted compound. Structures similar to those of pure CoTiSb are observed also for the substituted compounds. A remarkable shift of the peaks towards the Fermi energy ϵ_F is obtained for Sc substitution, whereas for V substitution a shift away from ϵ_F is observed. It is explained by the depletion or filling of states in the valence band when substituting Ti ($3d^2 4s^2$) by Sc ($3d^1 4s^2$) or V ($3d^3 4s^2$). In fact, ϵ_F is changed or—equivalently—the bands move towards or away from ϵ_F that is here the reference energy.

For a pure semiconducting compound the Fermi-energy is located at $T = 0$, by definition, at the highest occupied state that is the top of the valence band. Any small deviation $\delta \rightarrow \pm 0$ in the number of electrons will shift the Fermi energy in the spectra. Creation of holes ($\delta < 0$), indeed, keeps ϵ_F very close to the top of the valence band. In contrast, creation of electrons ($\delta > 0$) will cause a jump of ϵ_F to the bottom of the conduction band. From Figs. 5 and 7(b), it is evident that the CoTiSb sample is electron doped. Independent on the occurrence of in-gap states, ϵ_F is obviously located at the bottom of the conduction band. Substitution by V and thus further electron doping results in a only small shift of the steep onset of the d bands by about 150 meV as is expected from the VCA calculations. From the spectrum of $CoTi_{0.9}V_{0.1}Sb$, it is seen that the in-gap states survive the V substitution. The substitution by Sc and thus hole doping leads seemingly to much more drastic changes. Here, the onset of the d band jumps by about 1 eV towards zero and no in-gap states are recognized. This change of the spectrum is caused because the Fermi energy falls now into the valence band. The in-gap state, if still existing, may stay unoccupied and thus can not be detected anymore by photoelectron spectroscopy. A comparison to the calculations for Sc substitution with simultaneous antisite disorder (see Appendix B) hints that such a scenario is rather improbable as it would keep the Fermi energy inside of the band gap. It seems that the Sc substitution leads to a stabilization of the structure and reduces the probability of antisite disorder.

The electron filling and depletion is also seen from the shift of the major maxima in the spectra of the V and Sc substituted samples. The average shift is $\Delta E = 1.03 \pm 0.03$ eV. The differences in the spectra taken from $CoTi_{0.9}V_{0.1}Sb$ and $CoTi_{0.95}Sc_{0.05}Sb$ thus confirm that the size of the band gap is in the order of 1 eV in agreement to the *ab initio* calculations.

D. Vibrational and mechanical properties

The vibrational properties of CoTiSb were calculated by means of PHONON[48] on the basis of the results from WIEN2k. The primitive cell containing three atoms was enlarged to a cell with 12 distinguished atoms to calculate the Hellmann-Feynman forces for the phonon analysis. For these calculations, a force convergence criterion of 10^{-4} Rya_{0B}^{-1} was used in addition to the energy convergence criterion. Figure 8 shows the calculated phonon dispersion $h\nu(q)$ and the accompanied density of states $g(\omega)$ of CoTiSb. As expected for $C1_b$ structure with three atoms in the primitive cell, the phonon dispersion exhibits nine branches, three acoustic one longitudinal (LA) and two transversal (TA)] and six optical branches. A gap of about 4.4 meV between the acoustic and the optical branches is observed, due to the differences in the atomic masses of the atoms. The energies of the optical phonons at the Γ point are 28.4 and 32.2 meV, in perfect agreement with the absorption lines observed in the experiment as shown in Fig. 4(b).

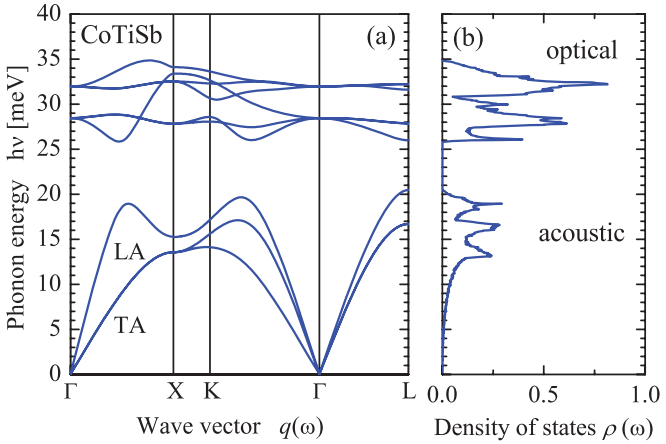

FIG. 8. (Color online) Phonon dispersion (a) and corresponding phonon density of states (b) of CoTiSb.

TABLE II. Mechanical properties of CoTiSb. Calculated elastic constants c_{ij} as well as the modulus are given in GPa; Poison's ratio (ν) and elastic anisotropy (A_e) are dimensionless quantities.

c_{11}	c_{12}	c_{44}	B	E	G	ν	A_e
259	84	93	142	224	91	0.24	1.06

The mechanical stability of thermoelectric materials is required to reach high efficiency and reliability of thermoelectric modules. Therefore the mechanical properties of CoTiSb were investigated. Details of the calculations have been reported in previous work.[36] The values of the calculated elastic constants c_{ij}, bulk modulus B, Young's modulus E, rigidity modulus G, Poison's ratio ν, and elastic anisotropy A_e are listed in Table II. The values of the calculated elastic constants as well as the elastic anisotropy A_e being close to unity satisfy the criteria for mechanical stability of CoTiSb in the cubic system.[49]

The elastic anisotropy $A_e = 2\,c_{44}/(c_{11} - c_{12})$ is close to unity that means that Young's modulus $E(\hat{r})$ exhibits a spherical distribution. For $A_e \leqslant 0$ or $A_e \to \infty$, the crystal would not be stable in the cubic structure as one of the Born-Huang criteria for stability ($c_{11} - c_{12} > 0$ or $c_{44} > 0$) is violated.[49] For $A_e > 1$, one finds that $E(\hat{r})$ is highest along the space diagonal ($\langle 111 \rangle$-type directions) whereas it is highest along the cubic axes ($\langle 001 \rangle$-type directions) for $1 > A_e > 0$.

Figure 9(a) compares the temperature dependence of the measured specific heat $C(T)$ to the calculated lattice specific heat $C_L(T)$. Below 100 K, $C(T)$ agrees well with $C_L(T)$, where at higher temperature the measured specific heat $C(T)$ is higher than $C_L(T)$, due to the contribution from electrons in the experimental $C(T)$. Both curves increases with increasing temperature and reach a value of about 9 k_B at high temperatures as expected from the Dulong-Petit law.

The Debye temperature Θ_D^{calc} or Θ_D^{exp} is found by fitting the calculated or measured specific heat to the Debye model, respectively. The results are shown in Fig. 9(b). The Debye temperature calculated from $C_L(T)$ is $\Theta_D^{\text{calc}} = 396.8$ K in the high-temperature limit ($T > 100$ K). This value is in good agreement with $\Theta_D^{\text{exp}} = 396.2$ K obtained from the measured specific heat $C(T)$.

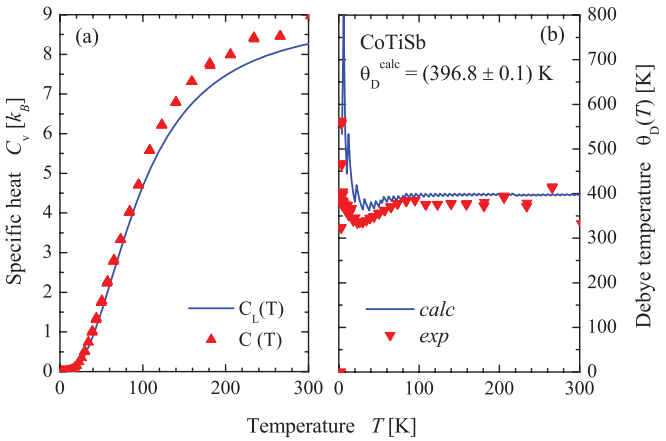

FIG. 9. (Color online) Specific heat (a) and Debye temperature (b) of CoTiSb. $C(T)$ is the measured specific heat and $C_L(T)$ is the calculated lattice specific heat.

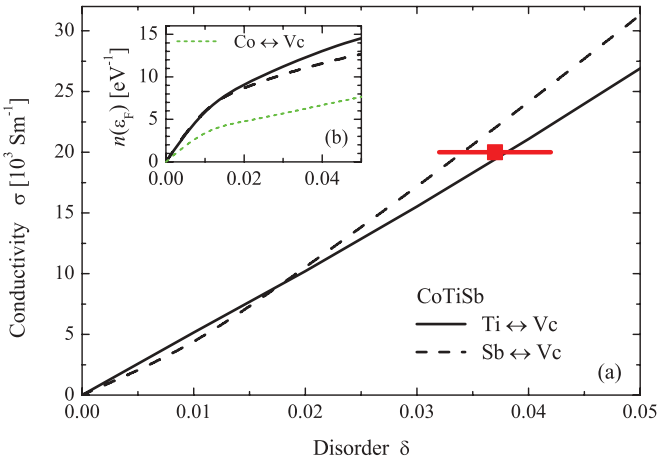

FIG. 10. (Color online) Calculated dependence of the electrical conductivity σ of CoTiSb on different types of disorder. δ is the number of swapped atom to the vacant position 4b. (b) shows the density of states at ϵ_F (the Co-Vc swap is given for comparison). The calculations were performed using KKR with CPA.

E. Transport properties

Due to the vacancy in the crystalline structure, $C1_b$ Heusler compounds are sensitive to antisite disorder, which may have a strong influence on the electronic structure, and consequently on the physical properties.[17,19,41,50] Therefore

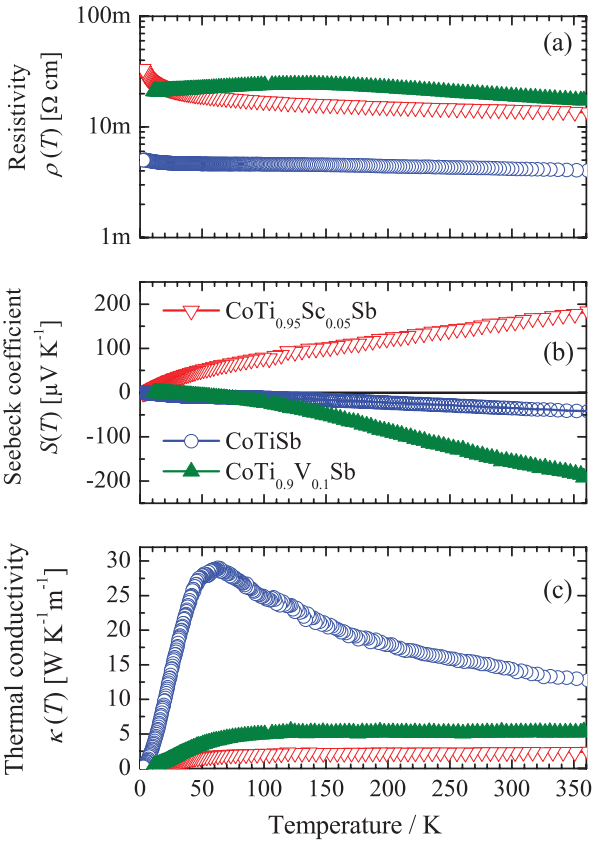

FIG. 11. (Color online) Temperature dependence of electrical resistivity $\rho(T)$, Seebeck coefficient $S(T)$, and thermal conductivity $\kappa(T)$ of CoTiSb, $CoTi_{0.95}Sc_{0.05}Sb$, and $CoTi_{0.9}V_{0.1}Sb$.

TABLE III. Thermal conductivity κ, Seebeck coefficient S, electrical conductivity σ, and figure of merit ZT of $CoTi_{1-x}M_xSb$ (M = Sc, V) at 350 K.

M	x [%]	κ [$WK^{-1}m^{-1}$]	S [μVK^{-1}]	σ [10^3 Sm^{-1}]	ZT
Sc	20	6.6	4	26.1	$1.9\ 10^{-5}$
Sc	5	2.4	178	7.3	0.034
Sc	2	3.5	131	15.5	0.027
	0	13	−35	20	0.001
V	1	4.5	−367	2.5	0.012
V	5	4.7	−163	6.7	0.013
V	10	5.2	−183	5.7	0.013

the electrical conductivity σ of different kinds of disorder in CoTiSb was calculated using KKR-CPA. The antisite disorder was modeled within CPA (details of the electronic structure for the substituted compounds including additional antisite disorder are explained in Appendix B). Figure 10(a) shows the calculated conductivity σ of disordered CoTiSb by swapped Sb or Ti atoms into the vacant position 4*b*. The density of states at the Fermi energy is drawn in the inset as function of the disorder level δ. The Co-Vc swap causes less states in the gap at ϵ_F, a noticeable conductivity was only found for $\delta > 5\%$. It is interesting to note that the Sb swap causes a faster increase of the conductivity compared to Ti, even though the density of states at the Fermi energy behaves opposite. The horizontal line at about 20×10^3 Sm^{-1} shows the measured conductivity of CoTiSb. For a disorder of 3.7% (as found from the refinement of the XRD data), the measured conductivity is in well agreement to the Ti↔Vc swap.

Figure 11 compares the temperature dependence of electrical resistivity $\rho(T)$, Seebeck coefficient $S(T)$, and thermal conductivity $\kappa(T)$ of pure CoTiSb to the substituted compounds $CoTi_{0.95}Sc_{0.05}Sb$ and $CoTi_{0.9}V_{0.1}Sb$. The electrical resistivity of the substituted compounds exhibits a semiconducting-type behavior and decreases with increasing temperature. The thermal conductivity $\kappa(T)$ of CoTiSb is high and exhibits a maximum at about 60 K, which is typical for well ordered compounds. By Sc or V substitution, a reduction of $\kappa(T)$ by about 30% is observed (see Table III). This reduction is caused by impurity scattering of phonons at the substituted atoms.

The Seebeck coefficient $S(T)$ of CoTiSb is negative with a value of -35 μV/K at room temperature. This value is lower compared to the previously reported Seebeck coefficients. Concerning previous works, the measured Seebeck coefficient and electrical conductivity of CoTiSb show mutually inconsistent values from -40 up to -265 μV/K for S (see Refs. 27 and 21), and from 1×10^3 to 3×10^3 S/m for σ (see Refs. 21 and 29). It is worthwhile to note, however, that both $S(T)$ and $\sigma(T)$ depend strongly on the synthesis procedures and post fabrication heat treatments.

The absolute value of $S(T)$ increases for V substitution. When substituting Ti by Sc the Seebeck coefficient reverses its sign such that the compound becomes p type in full agreement with the expectations from the calculations (see Fig. 13). Table III summarizes the behavior of thermal conductivity, Seebeck coefficient, electrical conductivity, and figure of merit of $CoTi_{1-x}M_xSb$ at 350 K with different amounts (x) of Sc and V substitution. At high Sc substitution (20%), the compound becomes metallic, as expected, and $S(T)$ decreases rapidly. The electrical conductivity of Sc substituted CoTiSb is higher that of the V substituted one, in contrast to the NiTiSn system.[41]

However, such differences in the properties depend critically on the element occupying the T and T' sites in the compounds, which play the main role in the behavior of the electronic band dispersion of the topmost valence or lowest conduction bands. To clarify the influence of the electronic structure on the electronic transport properties, the Fermi surfaces of $CoTi_{0.95}M_{0.05}Sb$ (M = Sc, V) were calculated using KKR-CPA. As mentioned above a band structure is not defined in nonperiodic structures but only the Bloch spectral function. The latter allows to project the number of states onto the Fermi surface. Figures 12(a) and 12(b) compares parts of the KKR-CPA Fermi surfaces in the Γ-X type planes of $CoTi_{0.95}Sc_{0.05}Sb$ and $CoTi_{0.95}V_{0.05}Sb$, respectively. These correspond to Fermi surface cross- sections in the (001) plane. The random site occupation leads to a

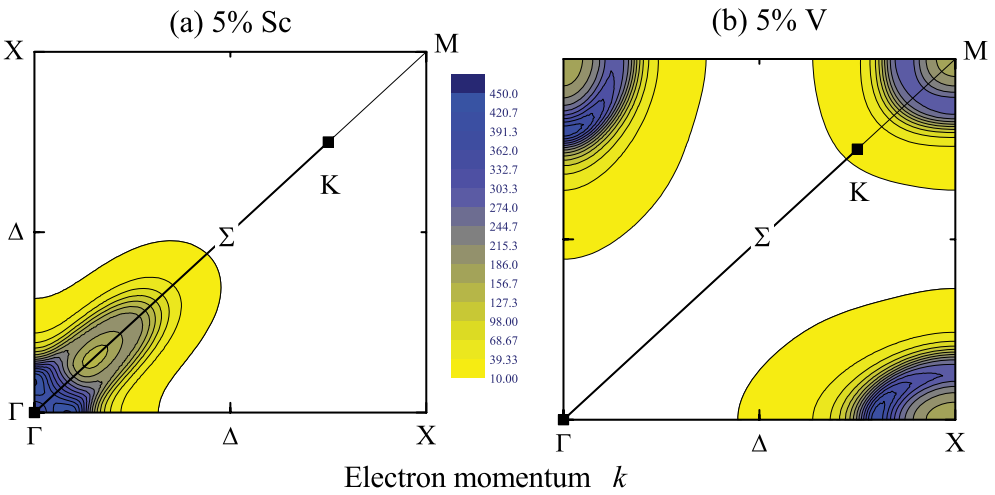

FIG. 12. (Color online) Cut through the Fermi surfaces of $CoTi_{0.95}M_{0.05}Sb$ for M = Sc (a) and V (b) in the (001) plane obtained from KKR-CPA calculations. The color (gray) scale corresponds to the number of states crossing the Fermi energy.

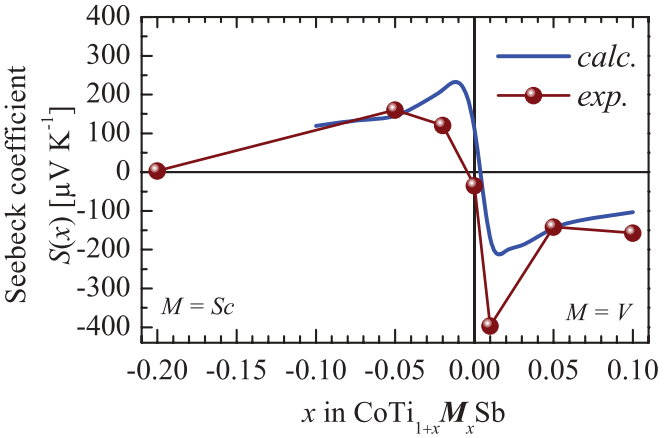

FIG. 13. (Color online) Calculated and measured Seebeck coefficient $S(T)$ of electron and hole doped CoTiSb. The values are given for $T = 300K$. The calculations were performed by Boltztrap using the results of the VCA electronic structure.

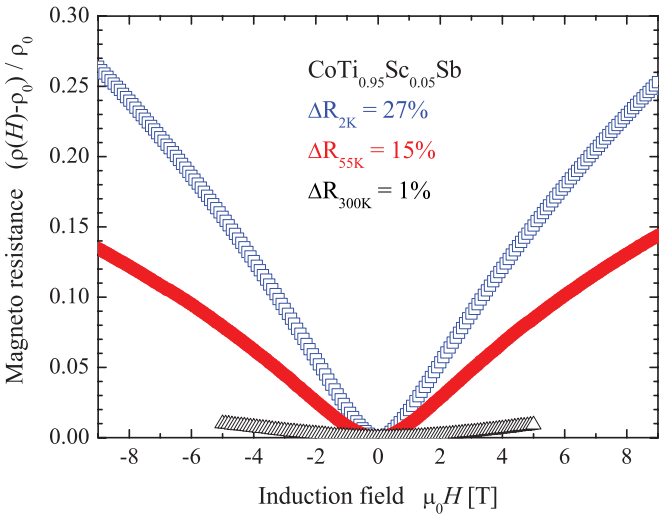

FIG. 14. (Color online) Magnetoresistance of $CoTi_{0.95}Sc_{0.05}Sb$ measured at different temperatures.

smearing of the states that cross the Fermi surface. The Fermi surface is populated around the Γ point for Sc substitution, whereas the population is largest around the X point for V substitution. One clearly has only one hole pocket at Γ for Sc but several electron pockets around X and K (M) for V for the different types of substitution. This difference indicates the importance of the band shapes and explains the high value of the measured electrical conductivity for the Sc substituted compound compared to the measured low values for V substitution. It is also clear that the Seebeck coefficient will not follow the simple approximation of the Mott equation[51,52] where it depends only on the change of the number of carriers through the logarithmic derivative of the density of states at ϵ_F.

The Seebeck coefficient was additionally calculated in VCA approach for different substitution as described in Sec. II. Figure 13 compares the measured and calculated Seebeck coefficients of Sc and V substituted CoTiSb at $T = 300$ K. The calculated Seebeck coefficient of CoTiSb is positive, whereas it is negative in the measurements. This difference in the sign is a direct consequence of the observed in-gap states that are not included in the calculations. For the substituted compounds, the general variation agrees qualitatively with the calculation. For 5% Ti substitution by Sc as well as V, the size and sign of the measured Seebeck coefficient agree well with the calculated values. This demonstrates that the influence of the in-gap states on the thermoelectric properties can be neglected at high substitution level.

F. Magnetoresistance

The magnetoresistance (MR) of the Sc substituted compound was measured in addition to the transport properties. A remarkable effect was found for $CoTi_{0.95}Sc_{0.05}Sb$ as seen from Fig. 14 that shows the measurement at three different temperatures. At room temperature, the MR is low and exhibits a week quadratic dependence on the applied magnetic field. At low temperature, the MR increases considerably and reaches a value of about 27% at a induction field of 9 T. Such a behavior may be the result of the impurity states in the hole pockets of the Fermi surface (see Fig. 12) created by the substitution. Ferromagnetic doping of $CoTi_{1-x}M_xSb$ by $M = Cr$ or Fe was already reported in previous work.[19] $CoTi_{0.95}Sc_{0.05}Sb$ is, indeed, not ferromagnetic, but interesting for magnetoelectronics because of the high magnetoresistance without magnetic stray fields. This makes the compounds suitable for spintronics or multifunctional devices.

V. SUMMARY

The Heusler compound CoTiSb was synthesized and investigated by experiments and first-principles calculations. The optical properties of CoTiSb were measured and compared to *ab initio* calculations. The complex permittivity shows a strong absorption peak at 1.83 eV that is in perfect agreement with the calculated size of the direct band gap at the Γ point. The optical absorption quickly drops to zero at lower energies, as expected for semiconductors when the photon energies become smaller than the gap size. The wide-range infrared reflectivity measurements exhibit strong absorption at a photon energy of 34 meV and weakly at 28 meV. These energies are in well agreements to the calculated energy of the optical phonons at the Γ point. The calculated vibrational and mechanical properties of CoTiSb prove the mechanical stability of the compound in the cubic $C1_b$ structure.

Furthermore, the properties of the solid solution series $CoTi_{1-x}M_xSb$ ($M = Sc$, V) were systematically studied. The thermal conductivity of the substituted compounds is effectively depressed (about 30%) by substitution of Ti by Sc or V. A 5% Sc substitution resulted in a p-type behavior with a high Seebeck coefficient of $+177.8\ \mu V/K$ at 350 K. This value is in good agreement with the calculations. The fully relativistic Korringa-Kohn-Rostoker (KKR) method in combination with the coherent potential approximation (CPA) was used to calculate the Fermi surface of $CoTi_{0.95}M_{0.05}Sb$ ($M = Sc$, V). The results showed that it is dominated by hole pockets a the Γ point for Sc and electron pockets at the X and K points for V substitution. These differences are responsible for the change of the transport properties of

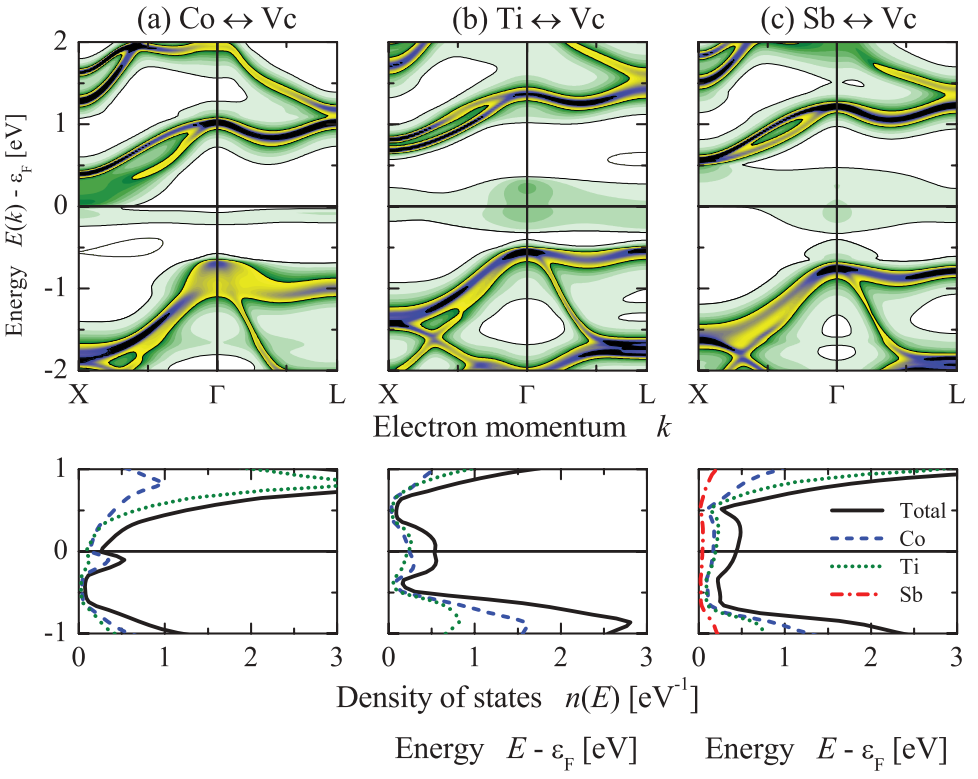

FIG. 15. (Color online) Electronic structure of CoTiSb with 5% M↔Vc antisite disorder for M = Co (a), Ti (b), and Sb (c). The upper panels (a), (b), and (c) show the Bloch spectral function in the high-symmetry directions Δ ($\Gamma - X$) and Λ ($\Gamma - L$). The bottom panels show the accompanied total and partial density of states calculated for the full Brillouin zone.

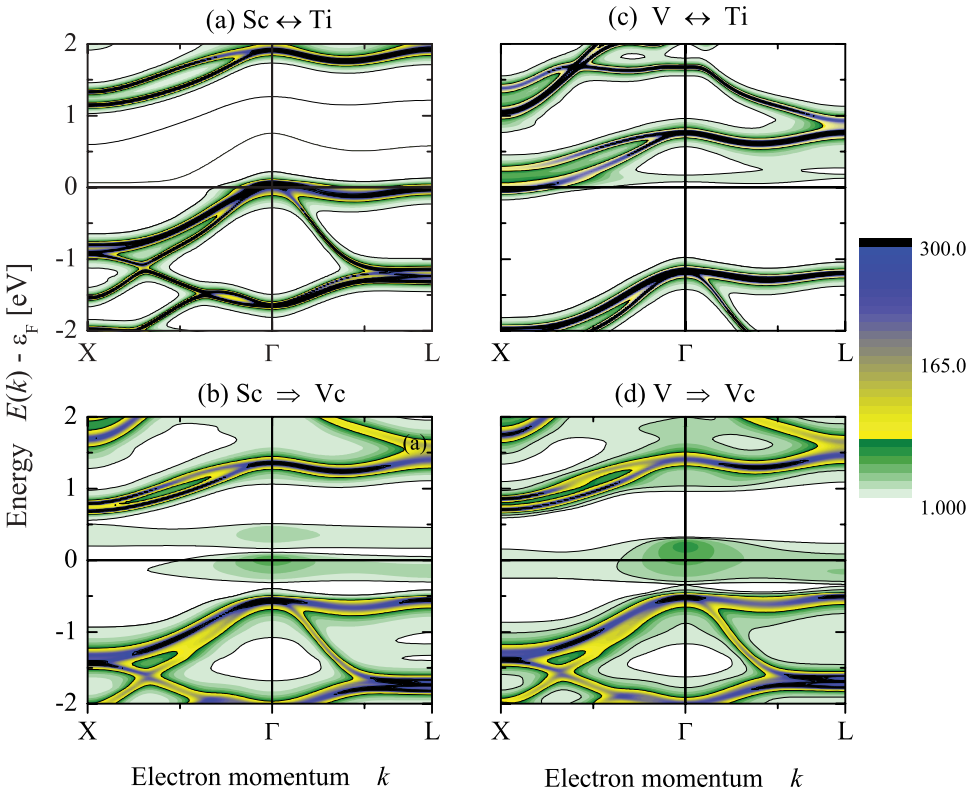

FIG. 16. (Color online) Bloch spectral function of $CoTi_{0.95}M_{0.05}Sb$ (M = Sc, V) in the Δ (Γ-X) and Λ (Γ-L) directions for M↔Ti (a) and (c) and M⇒Vc (b) and (d), respectively.

the compound for different type of substitution. A relatively high magnetoresistance of about 27% at 2 K was observed for $CoTi_{0.95}Sc_{0.05}Sb$. This makes the compounds a promising candidate not only for thermoelectric applications, but also for spintronics or multifunctional devices.

ACKNOWLEDGMENTS

The authors gratefully acknowledge financial support by the DfG (P 1.3-A in FOR 1464 ASPIMATT), DFG (Fe633/8-1 in SPP-1386) and and the Forschungszentrum Komplexe Materialien (COMATT, Johannes Gutenberg - University, Mainz). The HAXPES measurements were performed at BL15XU of SPring-8 with the approval of NIMS (Nanonet Support Proposal 2010A4903). The Ostrava group acknowledges financial support from PIEF-GA-2009-254511, CZ.1.05/1.1.00/02.0070, and CZ.1.07/2.3.00/20.0074.

APPENDIX A: CoTiSb ANTISITE DISORDER

In this appendix, some more details of the electronic structure of disordered CoTiSb are discussed. It was implied that the constituents swap partially into the vacant position of the $C1_b$ structure. In that case, the band structure is not longer defined due to the loss of periodicity in systems with random distribution of atoms. However, the Bloch spectral function and density of states can still be calculated from the Green's function. Figure 15 compares the Bloch spectral function for the two directions of highest rotational symmetry and density of states in the vicinity of the Fermi energy if the different types of atoms are swapped partially into the vacant site. For all three cases, a swap of 5% of the atoms was assumed. The results for other amounts between 1% and 10% are similar and 5% is a good compromise to make all important features easily visible. The compound may be written as Co□TiSb with Co, Ti, or Sb placed on the Wyckhoff positions 4a, 4c, or 4c and □ is the Wigner symbol for the vacancy on the 4b position. The disordered compounds are then written as $(Co_{1-x}\square_x)(\square_{1-x}Co_x)$TiSb and similar for the other cases to assign that the filling of the vacancy at the 4b site results in the creation of Co vacancies at 4a or similar on 4c or 4d for Ti or Sb swap that is $Co(\square_{1-x}Ti_x)(Ti_{1-x}\square_x)Sb$, or $Co(\square_{1-x}Sb_x)Ti(Sb_{1-x}\square_x)$, respectively. Atoms or vacancies on the same position are combined in brackets.

It is obvious from Fig. 15 that the different types of antisite disorder have different effects on the electronic structure. In all three cases, the compound becomes metallic with different types of in-gap states that appear inside of the initially semiconducting band gap. For Ti or Sb swap, the in-gap states appear concentrated at the Γ point creating a high density of states at ϵ_F. Co is considerably different, here the states appear stronger at the X point and the Fermi energy falls in a region with low density. This explains directly the differences in the effect of the type of disorder on the conductivity as shown in the main part in Fig. 10.

APPENDIX B: SUBSTITUTION WITH ANTISITE DISORDER

In the main part it was reported that Ti tends to antisite disorder and exhibits a small amount of swap into the vacant site. Principally, it can not be excluded that also part of the substituted atoms is occupying the vacant site instead of completely substituting the Ti. In general, this may lead to complicated situations. Therefore simplified calculations assuming that all substituted atoms occupy the vacant site were carried out in order to explain the influence of that type of disorder on the electronic structure and transport properties. In this case, the removed Ti leaves some part of the Ti site empty. Writing the compound as Co□TiSb the two situations are $Co\square(Ti_{1-x}M_x)Sb$ and $Co(\square_{1-x}M_x)(Ti_{1-x}\square_x)Sb$, where □ is the Wigner symbol for the vacancy and M = Sc or V.

Figures 16(a) and 16(c) show the Bloch spectral function if Sc or V substitute the Ti completely. The band gap is conserved and the Fermi energy is shifted into the valence or conduction band by the hole or electron doping, respectively. The situation changes if the substituted atoms do not occupy the Ti position but the vacant site. Even though one has still electron or hole doping, the Fermi energy is not shifted across the former band edges. Instead, the atoms in the vacant position lead again to creation of in-gap states where ϵ_F is pinned. As for the disordered compound (see above), the states are localized close to the Γ point similar to the cases of Ti-Vc or Sb-Vc antisite disorder. However, clear differences are observed comparing Sc and V on the vacant site. For Sc, a splitting of the states at ϵ_F is observed whereas a single state appears for V.

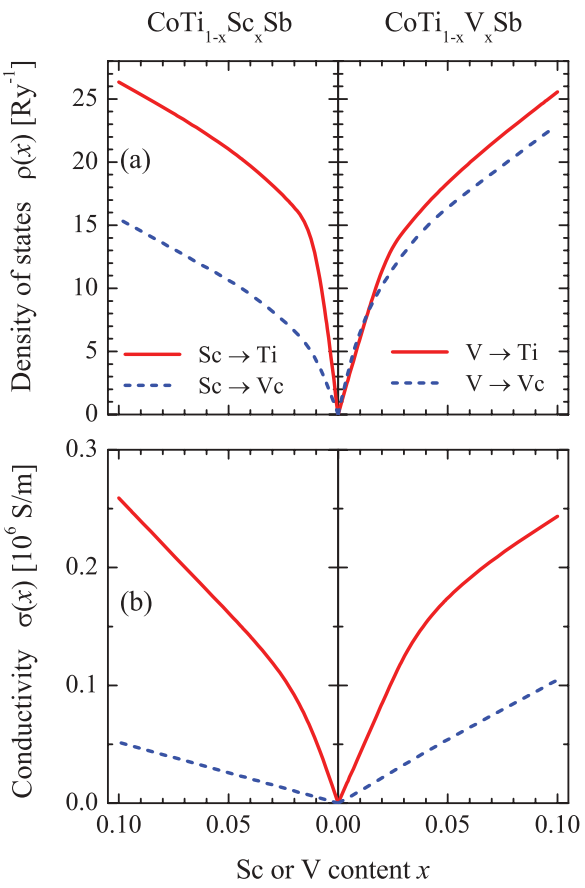

FIG. 17. (Color online) Calculated density of states (a) and corresponding conductivity σ (b) of $CoTi_{1-x}M_xSb$ (M = Sc, V). It was assumed that M substitutes Ti or occupies completely the vacant site leaving part of the Ti site unoccupied.

The obtained differences in the electronic structure should also influence the transport properties. Figure 17 shows the calculated electrical conductivity for the different cases. The direct substitution results in a higher conductivity compared to the case were the exchanged atoms occupy the vacant side. The reason is not only the higher density of states at the Fermi energy when it is shifted by the substitution into the valence or conduction bands but also the differences in the type of states. This becomes clear from the case of V where the in-gap states produce also a high density of states at ϵ_F but the conductivity stays still small and comparable to the case of Sc.

The variation of the conductivity depending on the site occupied by the substituted atoms is rather large. This may explain the rather large differences in the measured conductivities reported in literature. Indeed, any type of antisite disorder that appears together with the substitution used for electron or hole doping will not only influence the electrical conductivity but also the Seebeck coefficient.

*fecher@cpfs.mpg.de

[1] J. Tobola, J. Pierre, S. Kaprzyk, R. V. Skolozdra, and M. A. Kouacou, J. Phys.: Condens. Matter **10**, 1013 (1998).

[2] J. Tobola and J. Pierre, J. Alloys Compd. **296**, 243 (2000).

[3] R. A. de Groot, F. M. Müller, P. G. van Engen, and K. H. J. Buschow, Phys. Rev. Lett. **50**, 2024 (1983).

[4] S. Chadov, X. Qi, J. Kübler, G. Fecher, C. Felser, and S. Zhang, Nat. Mater. **9**, 541 (2010).

[5] J. Pierre, R. V. Skolozdra, J. Tobola, S. Kaprzyk, C. Hordequin, M. A. Kouacou, I. Karla, R. Currat, and E. Lelievre-Berna, J. Alloys Compd. **262-263**, 101 (1997).

[6] J. R. Sootsman, Angew. Chem. **48**, 8616 (2009).

[7] M. Schwall and B. Balke, Appl. Phys. Lett. **98**, 042106 (2011).

[8] M. A. Kouacou, J. Pierre, and R. V. Skolozdra, J. Phys.: Condens. Matter **7**, 7373 (1995).

[9] H. C. Kandpal, C. Felser, and R. Seshadri, J. Phys. D **39**, 776 (2006).

[10] L. P. Romaka, M. G. Shelyapina, Y. V. Stadnyk, D. Fruchart, E. K. Hlil, and V. A. Romaka, J. Alloys Compd. **416**, 46 (2006).

[11] G. H. Fecher, A. Gloskovskii, K. Kroth, J. Barth, B. Balke, C. Felser, F. Schäfer, M. Mertin, W. Eberhardt, S. Mähl, and O. Schaff, J. Electron Spectrosc. Relat. Phenom. **156-158**, 97 (2007).

[12] L. L. Wang, J. Phys. D **105**, 013709 (2009).

[13] P. Amornpitoksuk and S. Suwanboon, J. Alloys Compd. **462**, 267 (2008).

[14] J. Tobola, J. Alloys Compd. **383**, 328 (2004).

[15] T. Sekimoto, K. Kurosaki, H. Muta, and S. Yamanaka, J. Alloys Compd. **394**, 122 (2005).

[16] V. A. Romaka, Y. V. Stadnyk, P. Rogl, L. Akselrud, V. Davydov, V. Romaka, Y. Gorelenko, and A. Horyn, Ukr. J. Phys. **53**, 157 (2008).

[17] C. S. Lue, C. F. Chen, F.-K. Chiang, and M.-W. Chu, Phys. Rev. B **80**, 174202 (2009).

[18] K. Kroth, B. Balke, G. H. Fecher, V. Ksenofontov, C. Felser, and H. J. Lin, Appl. Phys. Lett. **89**, 202509 (2006).

[19] B. Balke, G. H. Fecher, A. Gloskovskii, J. Barth, K. Kroth, C. Felser, R. Robert, and A. Weidenkaff, Phys. Rev. B **77**, 045209 (2008).

[20] B. Balke, K. Kroth, G. H. Fecher, and C. Felser, J. Appl. Phys. **103**, 07D115 (2008).

[21] Y. Xia, V. Ponnambalam, S. Bhattacharya, A. L. Pope, S. J. Poon, and T. M. Tritt, J. Phys.: Condens. Matter **13**, 77 (2001).

[22] Y. Kawaharada, K. Kurosaki, H. Muta, M. Uno, and S. Yamanaka, J. Alloys Compd. **384**, 308 (2004).

[23] N. Tareuchi, K. Gosho, M. Hiroi, and M. Kawakami, Physica B **359-361**, 1183 (2005).

[24] T. Sekimoto, K. Kurosaki, H. Muta, and S. Yamanaka, J. Alloys Compd. **407**, 326 (2006).

[25] T. Sekimoto, K. Kurosaki, H. Muta, and S. Yamanaka, Jpn. J. Appl. Phys. **46**, L673 (2007).

[26] T. Wu, W. Jiang, X. Li, Y. Zhou, and L. Chen, J. Appl. Phys. **102**, 103705 (2007).

[27] M. Zhou, L. Chen, C. Feng, D. Wang, and J.-F. Li, J. Appl. Phys. **101**, 113714 (2007).

[28] P. Qiu, X. Huang, X. Chen, and L. Chen, J. Appl. Phys. **106**, 103703 (2009).

[29] T. Wu, W. Jiang, X. Li, S. Bai, S. Liufu, and L. Chen, J. Alloys Compd. **467**, 590 (2009).

[30] B. Balke, J. Barth, M. Schwall, G. H. Fecher, and C. Felser, J. Electron. Mater. **40**, 702 (2011).

[31] X. Yan, G. Joshi, W. Liu, Y. Lan, H. Wang, S. Lee, J. W. Simonson, S. J. Poon, T. M. Tritt, G. Chen, and Z. F. Ren, Nano Lett. **11**, 556 (2011).

[32] F. Aliev, F. Brandt, V. Moshchalkov, V. V. Kozyrkov, R. V. Skolozdra, and A. Belogorokhov, Z. Phys. B **75**, 167 (1989).

[33] Z. Popovic, K. G., R. Liu, and F. G. Aliev, Solid State Commun. **74**, 829 (1990).

[34] F. G. Aliev, Physica B **171**, 199 (1991).

[35] S. Ouardi, G. H. Fecher, C. Felser, J. Hamrle, K. Postava, and J. Pistora, Appl. Phys. Lett. **99**, 211904 (2011).

[36] S. Ouardi, G. H. Fecher, B. Balke, A. Beleanu, X. Kozina, G. Stryganyuk, C. Felser, W. Kloss, H. Schrader, F. Bernardi, J. Morais, E. Ikenaga, Y. Yamashita, S. Ueda, and K. Kobayashi, Phys. Rev. B **84**, 155122 (2011).

[37] B. Kong, X. R. Chen, J. X. Yu, and C. L. Cai, J. Alloys Compd. **509**, 2611 (2011).

[38] B. Kong, B. Zhu, Y. Cheng, L. Zhang, Q. X. Zeng, and X. W. Sun, Physica B **406**, 3003 (2011).

[39] P. Blaha, K. Schwarz, G. K. H. Madsen, D. Kvasnicka, and J. Luitz, *WIEN2k, An Augmented Plane Wave + Local Orbitals Program for Calculating Crystal Properties* (Karlheinz Schwarz, Techn. Universität Wien, Wien, Austria, 2001).

[40] G. K. H. Madsen and D. J. Singh, Comput. Phys. Commun. **175**, 67 (2006).

[41] S. Ouardi, G. H. Fecher, B. Balke, X. Kozina, G. Stryganyuk, C. Felser, S. Lowitzer, D. Ködderitzsch, H. Ebert, and E. Ikenaga, Phys. Rev. B **82**, 085108 (2010).

[42] J. P. Perdew, K. Burke, and M. Ernzerhof, Phys. Rev. Lett. **77**, 3865 (1996).

[43]H. Ebert, D. Ködderitzsch, and Minar, Rep. Prog. Phys. **74**, 096501 (2011).
[44]S. Ueda, Y. Katsuya, M. Tanaka, H. Yoshikawa, Y. Yamashita, S. Ishimaru, Y. Matsushita, and K. Kobayashi, AIP Conf. Proc. **1234**, 403 (2010).
[45]R. Brendel and D. Bormann, J. Appl. Phys. **71**, 1 (1992).
[46]S. Ouardi, G. H. Fecher, C. Felser, C. F. G. Blum, D. Bombor, C. Hess, S. Wurmehl, B. Büchner, and E. Ikenaga, Appl. Phys. Lett. **99**, 152112 (2011).
[47]S. Ouardi, C. Shekhar, G. H. Fecher, X. Kozina, G. Stryganyuk, C. Felser, S. Ueda, and K. Kobayashi, Appl. Phys. Lett. **98**, 211901 (2011).
[48]K. Parlinski, Z.-Q. Li, and Y. Kawazoe, Phys. Rev. Lett. **78**, 4063 (1997).
[49]M. Born and K. Huang, *Dynamical Theory of Crystal Lattices* (Clarendon Press, Oxford, 1956).
[50]S. Ouardi, G. H. Fecher, B. Balke, M. Schwall, X. Kozina, G. Stryganyuk, C. Felser, E. Ikenaga, Y. Yamashita, S. Ueda, and K. Kobayashi, Appl. Phys. Lett. **97**, 252113 (2010).
[51]N. F. Mott and H. Jones, *The Theory of the Properties of Metals and Alloys* (Clarendon Press, Oxford, 1936).
[52]J. M. Ziman, *Electrons and Phonons* (Oxford University Press, Oxford, 1960).